JCB Article

The intranuclear mobility of messenger RNA binding proteins is ATP dependent and temperature sensitive

Alexandre Calapez,[1,4] Henrique M. Pereira,[2] Angelo Calado,[1] José Braga,[1] José Rino,[1] Célia Carvalho,[1] João Paulo Tavanez,[1] Elmar Wahle,[3] Agostinho C. Rosa,[4] and Maria Carmo-Fonseca[1]

[1]Instituto de Medicina Molecular, Faculdade de Medicina, Universidade de Lisboa, 1649-028 Lisboa, Portugal
[2]Department of Biological Sciences, Stanford University, Stanford, CA 94305
[3]Universität Halle, Institut für Biochemie, 06120 Halle, Germany
[4]Instituto de Sistemas e Robótica, Instituto Superior Técnico, 1049-001 Lisboa, Portugal

After being released from transcription sites, messenger ribonucleoprotein particles (mRNPs) must reach the nuclear pore complexes in order to be translocated to the cytoplasm. Whether the intranuclear movement of mRNPs results largely from Brownian motion or involves molecular motors remains unknown. Here we have used quantitative photobleaching techniques to monitor the intranuclear mobility of protein components of mRNPs tagged with GFP. The results show that the diffusion coefficients of the poly(A)-binding protein II (PABP2) and the export factor TAP are significantly reduced when these proteins are bound to mRNP complexes, as compared with non-bound proteins. The data further show that the mobility of wild-type PABP2 and TAP, but not of a point mutant variant of PABP2 that fails to bind to RNA, is significantly reduced when cells are ATP depleted or incubated at 22°C. Energy depletion has only minor effects on the intranuclear mobility of a 2,000-kD dextran (which corresponds approximately in size to 40S mRNP particles), suggesting that the reduced mobility of PABP2 and TAP is not caused by a general alteration of the nuclear environment. Taken together, the data suggest that the mobility of mRNPs in the living cell nucleus involves a combination of passive diffusion and ATP-dependent processes.

Introduction

How mRNAs travel from the site of transcription to the nuclear pores remains poorly understood. Immediately upon synthesis, nascent transcripts associate with proteins to form large ribonucleoprotein complexes (messenger ribonucleoprotein particles [mRNPs]*), the protein content of which evolves as pre-mRNA is processed into mRNA and nuclear mRNA is exported to the cytoplasm (for recent reviews see Nakielny and Dreyfuss, 1999; Maquat and Carmichael, 2001). For several years, it was thought that the intranuclear environment was quite viscous and, consequently, the diffusion of large macromolecular complexes such as mRNPs was expected to be too slow (Agutter and Taylor, 1996). Based on this assumption, Blobel proposed the so-called gene gating hypothesis, which postulated a localized vectorial transport of mRNA toward the nuclear pores (Blobel, 1985). However, more recent measurements of the movement of molecules in the nucleus using photobleaching and fluorescence correlation spectroscopy techniques have indicated that macromolecule-sized solutes can diffuse in the nucleus at rates that are only approximately three- to fourfold slower than those observed in aqueous solution (Seksek et al., 1997; Politz et al., 1998). Most important, two recent reports addressing specifically the movement of nuclear mRNAs revealed properties that are characteristic of a random diffusive process (Politz et al., 1999; Singh et al., 1999). In the first study, nuclear poly(A) RNA was visualized in living cells by hybridization with an oligo(dT) probe labeled with chemically masked (caged) fluorescein (Politz et al., 1999). Upon unmasking the fluorescence by laser spot photolysis, the spread of the signal was followed by time-lapse microscopy. The second study used *Chironomous tentans* salivary gland cells (Singh et al., 1999). Newly synthesized RNA was labeled in vivo with BrUTP, the cells were fixed at sequential time points after the pulse, and the position

Address correspondence to Maria Carmo-Fonseca, Instituto de Medicina Molecular, Faculdade de Medicina, Avenida Prof. Egas Moniz, 1649-028 Lisboa, Portugal. Tel.: 351-21-7934340. Fax: 351-21-7951780. E-mail: carmo.fonseca@fm.ul.pt

A. Calapez and H.M. Pereira contributed equally to this work.

A. Calado's present address is Institut für Biochemie, ETH Zentrum, 8092 Zürich, Switzerland.

*Abbreviations used in this paper: FLIP, fluorescence loss induced by photobleaching; IPB, immunopurification buffer; mRNP, messenger ribonucleoprotein particle; PABP2, poly(A)-binding protein II.

Key words: mRNA; PABP2; TAP; nucleus; photobleaching

of labeled Balbiani ring particles in the nucleus was analyzed by immunoelectron microscopy.

In the present work, GFP was fused to two distinct mRNP-binding proteins (poly[A]-binding protein II [PABP2] and TAP) and the mobility of the tagged complexes was analyzed by quantitative photobleaching techniques. PABP2 binds to the growing poly(A) tails formed at the 3′ ends of nearly all eukaryotic mRNAs (Wahle, 1991). PABP2 cooperates with the cleavage and polyadenylation specificity factor to stimulate the activity of poly(A) polymerase, the enzyme that catalyses polyadenylation. The cleavage and polyadenylation reactions are currently thought to be coupled to splicing of the last intron and to occur at the same time as, or just before, transcription termination (Bauren et al., 1998; Dye and Proudfoot, 1999, 2001). This implies that GFP–PABP2 will bind to nearly terminated and spliced transcripts. Because not all poly(A) RNA is exported from the nucleus, we aimed at achieving a more specific visualization of mRNAs in transit to the cytoplasm by using GFP fused to the export factor TAP. TAP binds directly to the constitutive transport element of viral RNAs and is required for the nucleo-cytoplasmic export of cellular mRNAs in vertebrates, *Caenorhabditis elegans*, and *Saccharomyces cerevisiae* (for reviews see Görlich and Kutay, 1999; Nakielny and Dreyfuss, 1999; Conti and Izaurralde, 2001).

Here we have analyzed the effect of energy depletion on the intranuclear mobility of mRNP complexes tagged with GFP–PABP2 and GFP–TAP. For comparison, we determined the mobility rates of large dextrans microinjected into the nucleus of cells depleted of ATP or incubated at 22°C. The results suggest that energy-dependent processes influence specifically the traffic of mRNPs in the living cell nucleus.

Results

GFP–PABP2 assembles into mRNPs

We have previously shown that the GFP–PABP2 fusion protein colocalizes with endogenous PABP2, i.e., it is distributed throughout the nucleoplasm with a higher concentration in "speckles" (Calado and Carmo-Fonseca, 2000; Calado et al., 2000). Immunoblotting analysis of total proteins from cells expressing GFP–PABP2 using an anti-GFP antibody showed a single protein band, thus excluding the presence of truncated GFP chimeras. As depicted in Fig. 1 (lane 1), the GFP–PABP2 fusion protein is detected above the expected apparent molecular weight (~60 kD), reflecting the typical aberrant migration properties of PABP2 (Krause et al., 1994; Nemeth et al., 1995).

To determine whether GFP–PABP2 assembles into mRNP complexes, coimmunoprecipitation experiments were performed using nuclear extracts prepared from transfected cells. The binding properties of wild-type PABP2 were compared with those of a mutant variant, PABP2dm, which contains a double point mutation (a tyrosine to alanine at position 175 and a phenylalanine to alanine at position 215) in the RNA binding domain of the protein (Calado et al., 2000). Fig. 1 (lane 6) shows that a monoclonal antibody specific to hnRNP C (a protein that binds nascent transcripts; Dreyfuss et al., 1993) coprecipitates GFP–PABP2. This is no longer observed when extracts are treated with RNase A (Fig. 1, lane 7), indicating that coprecipitation results from independent binding of both hnRNP C and GFP–PABP2 to mRNA. As expected, a fusion of GFP with the dm variant of PABP2, which shows reduced binding affinity to poly(A) in vitro, fails to coprecipitate with hnRNP C in the absence of RNase treatment (Fig. 1, lane 8). Taken together, these results indicate that GFP–PABP2 binds to mRNA and assembles into mRNP complexes in vivo, whereas the mutant GFP–PABP2dm does not.

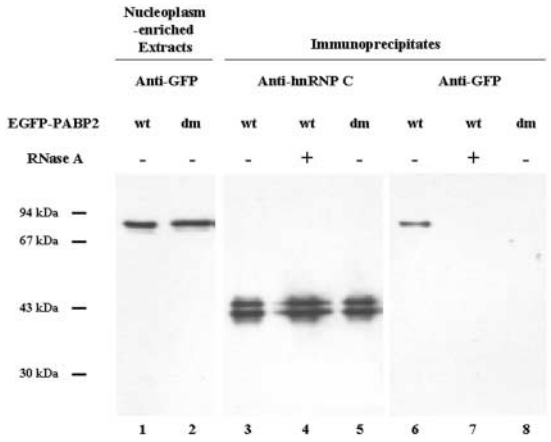

Figure 1. **GFP–PABP2 assembles into mRNP complexes.** Nucleoplasm-enriched extracts were prepared from HeLa cells expressing either wild-type (wt) or a mutant variant of PABP2 defective for poly(A) binding (dm). Total proteins from these extracts were probed with anti-GFP antibody (lanes 1 and 2). Immunoprecipitates obtained with the monoclonal antibody 4F4 (specific for hnRNP C proteins) covalently bound to protein A–Sepharose beads were probed with either anti–hnRNP C (lanes 3–5) or anti-GFP antibodies (lanes 6–8). When indicated (lanes 4 and 7), extracts were treated with RNase A before immunoprecipitation. Molecular weight markers (Amersham Biosciences) are displayed on the left side.

Kinetics of GFP–PABP2

Having established that mRNP complexes can be tagged by GFP–PABP2, we next performed FRAP experiments to analyze their mobility in the nucleus of living HeLa cells. A defined area in the nucleoplasm was bleached irreversibly by a single, high-powered spot laser pulse. The recovery of fluorescence signal in the bleached area, which is a consequence of the movement of nonbleached molecules into that region, was recorded by time-lapse imaging (Fig. 2).

Contrasting with the results observed in living cells (Fig. 2 B), there is no recovery of fluorescence after bleaching chemically fixed cells (Fig. 2 A). By several criteria, the bleach pulse does not induce cytotoxic effects. First, the bleached cells showed no signs of reduced vitality when stained with rhodamine 123, a fluorescent dye that is rapidly and specifically sequestered by active mitochondria (Fig. 2 C). Second, the recovery of fluorescence signal was not affected by repeated bleaching of the same nuclear region (Fig. 2 D). Third, bleached cells continued to divide (unpublished data).

For quantitative studies, we selected cells containing the minimal detectable level of GFP fusion proteins in order to avoid potential artifacts caused by overexpression. To monitor the expression level of GFP fusion proteins, the fluorescence intensity of each transfected nucleus was determined

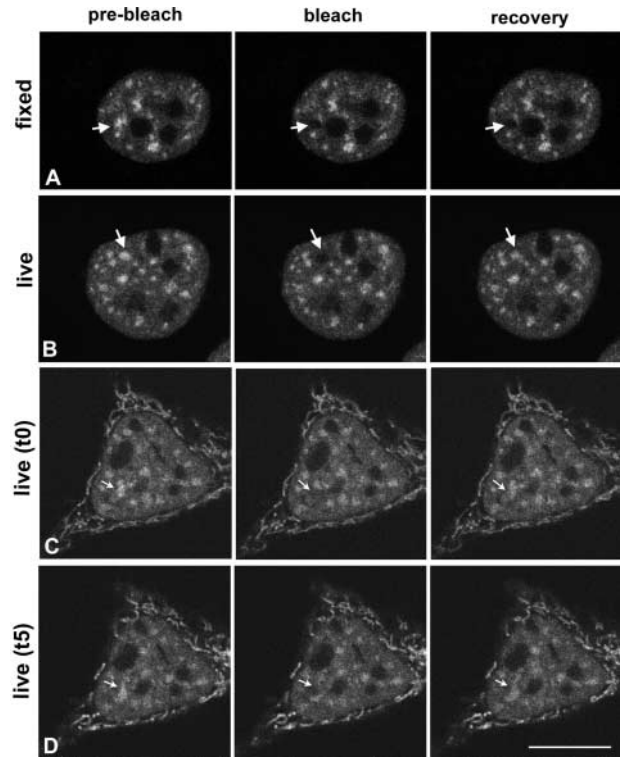

Figure 2. **FRAP of GFP–PABP2.** Cells expressing GFP–PABP2 were imaged before and during recovery after bleaching a spot in the nucleus (arrows). Note that the bleached region includes a nuclear speckle. The first image was taken immediately after the end of the bleach pulse. The recovery image was taken at either 7 (A and B) or 5 s (C and D) after bleaching. The cell depicted in A was fixed in 3.7% formaldehyde for 10 min, whereas all other cells were imaged alive. In C and D, which depict the same cell, active mitochondria are selectively stained with rhodamine 123. The indicated nuclear region was bleached and imaged 5 s later (C, arrows). After 5 min, the same nuclear region was again bleached and imaged 5 s later (D, arrows). Bar, 10 μm.

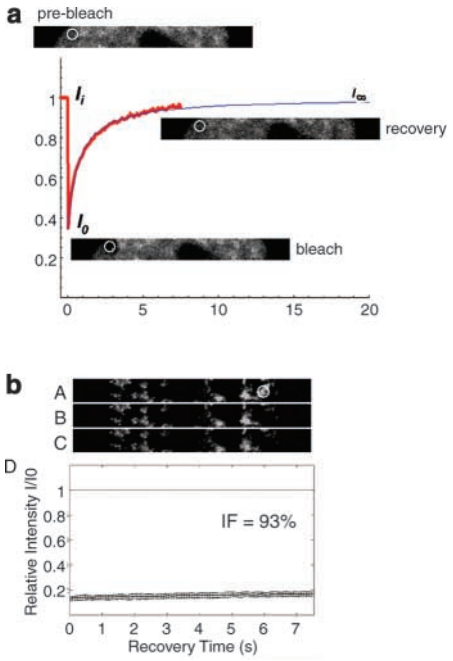

Figure 3. **Quantitative FRAP of GFP–PABP2.** (a) Cells expressing GFP–PABP2 were imaged before and during recovery after bleaching a spot in the nucleus (white circle). Note that the bleached region excludes any nuclear speckles. A plot of fluorescence intensity (I) as a function of time shows the parameters of a quantitative FRAP experiment. The recovery curve depicted (red) corresponds to a pool of four independent experiments, with 10 different cells analyzed per experiment. The bleach region is imaged during a prebleach period to determine the initial intensity I_i. This region is then bleached using high-intensity laser power. As a result, the fluorescence intensity decreases from the initial value I_i to I_0. Recovery is monitored starting at time t_0 until I reaches a final value or plateau, when no further increase can be detected (I_∞). I is corrected for the background intensity and the amount of total fluorescence lost during the bleach and imaging. The mobile fraction is the proportion of fluorescence that is regained, whereas the immobile fraction is calculated by comparing I_i and I_∞. For each experiment, the FRAP recovery curves are fitted to the recovery function (blue). Fitting of this function allows an estimation of immobile pools even when the recovery of the fluorescence intensity has not reached a plateau during the time of the experiment. (b) A chimera formed by fusion of PABP2 with coilin is immobile in the nucleus. Cells expressing GFP–PABP2 fused to an NH_2-terminal fragment of p80 coilin (amino acids 1–468) were imaged before (A), immediately after (B), and 7 s after bleaching (C). The fluorescence intensity in the bleached region was measured over time and expressed as the relative recovery (D). The recovery curve corresponds to a pool of three independent experiments, with 10 different cells analyzed per experiment. Error bars represent standard deviations. IF, immobile fraction.

using the same detection parameters as those applied during the imaging stage of photobleaching experiments. Because a fraction of poly(A) RNA appears to be retained in the nucleus, where it accumulates in so-called nuclear speckles or clusters of interchromatin granules (Huang et al., 1994), these domains were systematically excluded in all photobleaching measurements.

Quantitative FRAP yields information about the relative mobility of the fluorophore: the effective diffusion coefficient (D) and the fraction of fluorophore that is mobile (White and Stelzer, 1999; Reits and Neefjes, 2001). D indicates the surface area randomly sampled by the fluorophore in a given time, whereas the mobile fraction indicates how much of the fluorophore is available for recovery. To derive both D and the mobile/immobile fractions, the recovery of relative fluorescence intensity within the bleach region is plotted as a function of time (Fig. 3 a, red staining). A function is then fitted to this curve (Fig. 3 a, blue staining). GFP fusion proteins are considered to have a high mobility if they have both a high D and a high mobile fraction.

In clear contrast to the high mobility of GFP–PABP2, a chimera formed by fusing GFP–PABP2 to the Cajal body protein p80 coilin is predominantly immobile in the nucleus (Fig. 3 b). Although the mechanism underlying this immobilization is unknown, absence of recovery after photobleaching a nuclear region in cells expressing the GFP–PABP2–coilin chimera excludes the possibility that the fluorescence recovery is a consequence of GFP refolding or de novo synthesis.

For comparison purposes, we analyzed cells expressing GFP, which moves relatively freely throughout the nucleus and cytoplasm. In these cells, the fluorescence signal recovers to the prebleach value in <1 s (Fig. 4 A), and a similar behavior is observed in cells expressing GFP–PABP2dm, the mutant form of PABP2 with impaired ability to bind

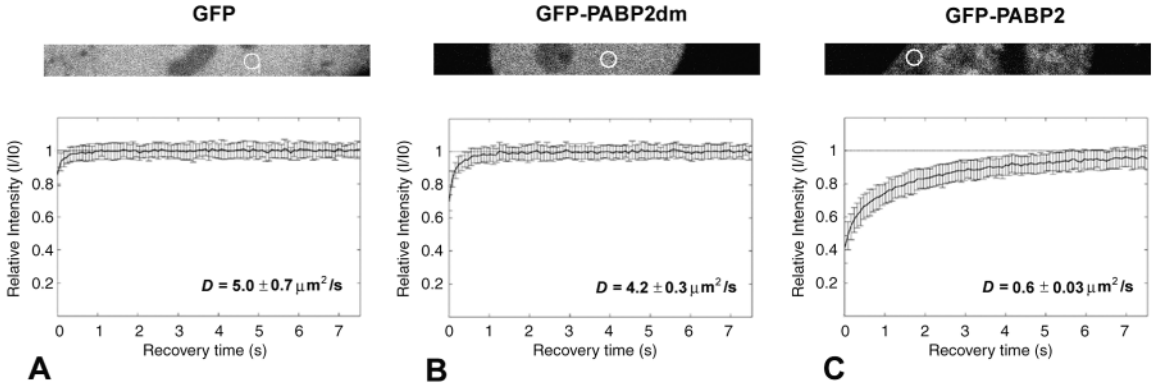

Figure 4. **FRAP kinetics of GFP–PABP2 and GFP–PABP2dm.** Cells expressing GFP (A), GFP–PABP2dm (B), or GFP–PABP2 (C) were imaged before and during recovery after bleaching. The area of the bleach spot is indicated with a circle (1.42 μm in diameter). The recovery curves correspond to a pool of three to five independent experiments, with 10 different cells analyzed per experiment. Error bars represent standard deviations. *D* values represent mean ± SEM.

poly(A) RNA (Fig. 4 B). In contrast, GFP–PABP2 requires >7 s to recover completely (Fig. 4 C). The calculated *D* value for GFP–PABP2 is 0.6 $\mu m^2 s^{-1}$, whereas for the mutant it is 4.2 $\mu m^2 s^{-1}$. This indicates that the kinetics of wild-type GFP fusion molecules is approximately sevenfold slower than mutant proteins. Taking into account that both wild-type and mutant GFP fusion proteins have the same molecular size but differ in their ability to bind to poly(A) RNA, the retardation of GFP–PABP2 molecules is most likely a consequence of binding to mRNP complexes.

To determine what fraction of GFP–PABP2 in the nucleus is actually bound to mRNP complexes, we next performed fluorescence loss induced by photobleaching (FLIP) experiments in cells expressing either GFP–PABP2 or GFP–PABP2dm (Fig. 5). To perform FLIP, a region in the nucleus was repeatedly bleached using high laser intensity while the surrounding area was imaged between each round of bleaching. The loss of fluorescence in the area outside of the bleached region is plotted over time, providing information on the rate of displacement of the molecules from that particular space. Repetitive bleaching of a defined nucleoplasmic area for 1,000 s leads to a loss of >95% of the initial fluorescence. Kinetic analysis of FLIP data for cells expressing low levels of GFP–PABP2 revealed the existence of a single slow moving population (Fig. 5 A), indicating that the vast majority of the fusion protein is bound to RNA. In cells expressing higher levels of GFP–PABP2 (Fig. 5 B), the analysis reveals two populations, one slow (with kinetics similar to that detected in low-level expressing cells) and one faster. The fraction of molecules in the faster population increased proportionately to the expression level of GFP–PABP2 (unpublished data), suggesting that it represents a pool of excessive proteins unbound to RNA. Kinetic analysis of FLIP data for GFP–PABP2dm showed the same two populations, but with a clear predominance of molecules with faster kinetics (Fig. 5 C). The additional presence of a minor (~28%) slow population is consistent with biochemical data indicating that the dm mutation significantly decreases, but does not entirely abolish, the ability of the protein to bind to RNA (Calado et al., 2000). Taken together, the data suggest that the FRAP recovery curves of GFP–PABP2 in cells expressing low levels of the fusion protein reflect the mobility of mRNP complexes in the living cell nucleus.

Comparing the intranuclear mobility of GFP–PABP2 and large dextrans

Electron microscopy of mRNPs isolated from mammalian cell nuclei reveal a repeating subunit structure of spherical particles connected by ribonuclease-sensitive strands (for review see Georgiev, 1981). Each monomer particle sediments in sucrose gradients at 30–40S, has a molecular weight of 1–2 × 10^6 D, and contains ~900 ribonucleotides (Pederson, 1974;

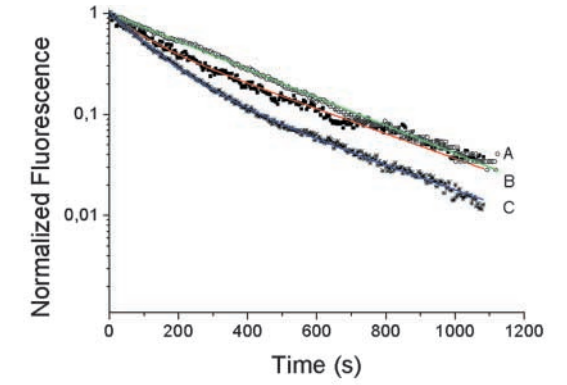

	p	R1	R2	χ2
A	1	0,00334 ±8,3823E-6	N/A	0,00012
B	0,61410 ±0,03148	0,00280 ±0,00009	0,01090 ±0,00085	0,00047
C	0,28715 ±0,01504	0,00264 ±0,00008	0,00852 ±0,00014	0,00005

Figure 5. **FLIP kinetics of GFP–PABP2 and GFP–PABP2dm.** Semi-logarithmic plots of nuclear loss of fluorescence in FLIP experiments performed on HeLa cells expressing GFP–PABP2 (A and B) and GFP–PABP2dm (C). Fitting functions are plotted in color. In A, a single exponential fit ($f(t) = Exp(-R\,t)$) shows the existence of a single population of slow moving GFP–PABP2. (B) A cell expressing a higher level GFP–PABP2 (higher absolute fluorescence intensity) can be fitted by a nonlinear function ($f(t) = p\exp(-R_1 t) + (1 - p)\exp(-R_2 t)$) that reveals the same slow population with an abundance of ~60% and a faster one with a rate constant three times higher. In C, a cell expressing GFP–PABP2dm was fitted with the same nonlinear function, and the same populations of slow and fast proteins are detected. Contrasting to the situation shown in B, the faster population is the most abundant (~70%).

Beyer et al., 1977; Georgiev, 1981). As the majority of HeLa mRNA averages 1,500 bases (Derman et al., 1976), the estimated average size of mRNP is in the range of 2–4 $\times$ 10^6 D.

To compare the nuclear mobility of GFP–PABP2 bound to RNP complexes with that of exogenous particles with similar size, FRAP experiments were performed on cells microinjected in the nucleus with fluorescein-labeled dextrans of 0.58 and 2 $\times$ 10^6 D. These probes, which are not degraded or metabolized by cells, have been previously used for photobleaching recovery measurements within the nucleus (Seksek et al., 1997). The estimated D value for the 580-kD dextran is 0.95 $\mu m^2 s^{-1}$, whereas for the 2,000-kD dextran, D is 0.53 $\mu m^2 s^{-1}$ (Fig. 6). In both cases, the recovery was incomplete, with immobile pools of 5 and 14%, respectively. This implies that Brownian motion is insufficient to sustain constant movement of large particles within the size range of mRNPs. Thus, the finding that poly(A) RNP complexes tagged with GFP–PABP2 are completely mobile in the nucleus (immobile fraction is 0%) argues that mRNP movement involves more than simple diffusional processes.

Energy depletion affects specifically for the mobility of wild-type GFP–PABP2

To investigate whether the difference observed between the intranuclear mobility of large dextrans and poly(A) RNP complexes tagged with GFP–PABP2 involves energy consumption, FRAP experiments were performed on cells depleted of ATP or incubated at a reduced temperature (22°C). To lower the cellular ATP levels, the cells were incubated with 2-deoxy-glucose and sodium azide. Within 5–10 min after treatment, most cells lost the staining with rhodamine 123, indicating that their mitochondria were no longer active (Fig. 7, A and B). As an additional control, we tested the effect of the energy depletion assay on receptor-mediated transport between the nucleus and the cytoplasm, as it is well established that this process is energy dependent (for review see Görlich and Kutay, 1999). Cells were transfected with GFP fused to a classical NLS (the SV40 large T antigen NLS). GFP is a small protein (~27 kD) that diffuses across the pores. However, due to the presence of an NLS, it is actively imported. Consequently, under physiological conditions, GFP–NLS is predominantly detected in the nucleus. When cells expressing GFP–NLS are incubated at 4°C, the fluorescence signal is detected both in the nucleus and in the cytoplasm because GFP–NLS diffuses passively to the cytoplasm and NLS-mediated transport to the nucleus is blocked (Fig. 7 C). Within 1 h after shifting the cells to 37°C, the fluorescence is again predominantly localized in the nucleus (Fig. 7 D). However, when cells are incubated at 22°C, the fluorescence remains in the cytoplasm (Fig. 7 E). Similarly, incubation at 37°C in the presence of D-glucose and azide is unable to restore import of GFP–NLS into the nucleus against its concentration gradient (Fig. 7 F).

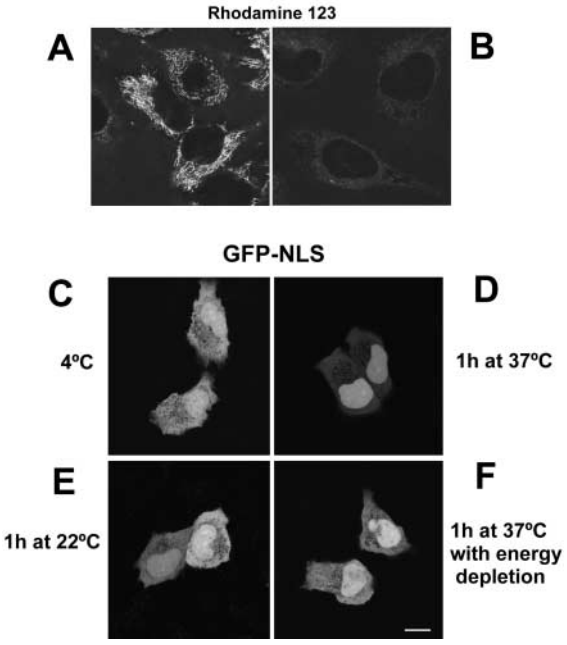

Figure 7. **Energy depletion blocks receptor-mediated nucleocytoplasmic transport.** Under physiological conditions, rhodamine 123 is selectively sequestered by active mitochondria (A). Within 5–10 min after treatment with D-glucose and sodium azide, the staining is abolished, indicating mitochondrial failure (B). To test the effect of energy depletion on receptor-mediated transport between the nucleus and the cytoplasm, cells were transfected with GFP fused to a classical NLS. When cells expressing GFP–NLS are incubated for 1–2 h at 4°C, the fluorescence signal is detected both in the nucleus and in the cytoplasm (C). Within 1 h after shifting the cells to 37°C, the fluorescence is predominantly localized in the nucleus (D). Cells incubated at either 22°C (E) or at 37°C in the presence of D-glucose and azide (F) are unable to restore import of GFP–NLS into the nucleus against its concentration gradient. Bar, 10 μm.

As illustrated in Fig. 8, when cells were either incubated at 22°C or ATP depleted, the diffusion coefficient of GFP–PABP2 was reduced from 0.6 $\mu m^2 s^{-1}$ to 0.2 $\mu m^2 s^{-1}$, which corresponds to ~30% of the control value. Because energy depletion treatments may alter the intranuclear environment and consequently affect diffusion rates in an indirect and unspecific manner, we analyzed the recovery curves of the 2,000-kD dextran and GFP–PABP2dm in cells that were either incubated at 22°C or ATP depleted (Fig. 8). At 22°C, the diffusion coefficient of both GFP–PABP2dm and the large dextran were reduced from 4.2 and 0.5 $\mu m^2 s^{-1}$ to 3.2–3.7 and 0.4–0.5 $\mu m^2 s^{-1}$, respectively. These values correspond to 75–77% of the D values at 37°C. In contrast to the temperature effect, ATP depletion did not affect the D value

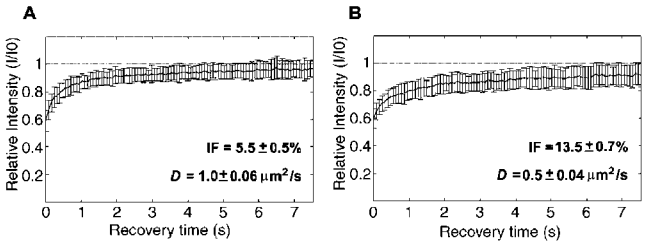

Figure 6. **FRAP kinetics of FITC–dextrans.** Cells were microinjected in the nucleus with FITC–dextrans of 580 and 2,000 kD. The recovery curves correspond to a pool of four independent experiments, with 10 different cells analyzed per experiment. Error bars represent standard deviations. IF, immobile fraction. D values represent mean ± SEM.

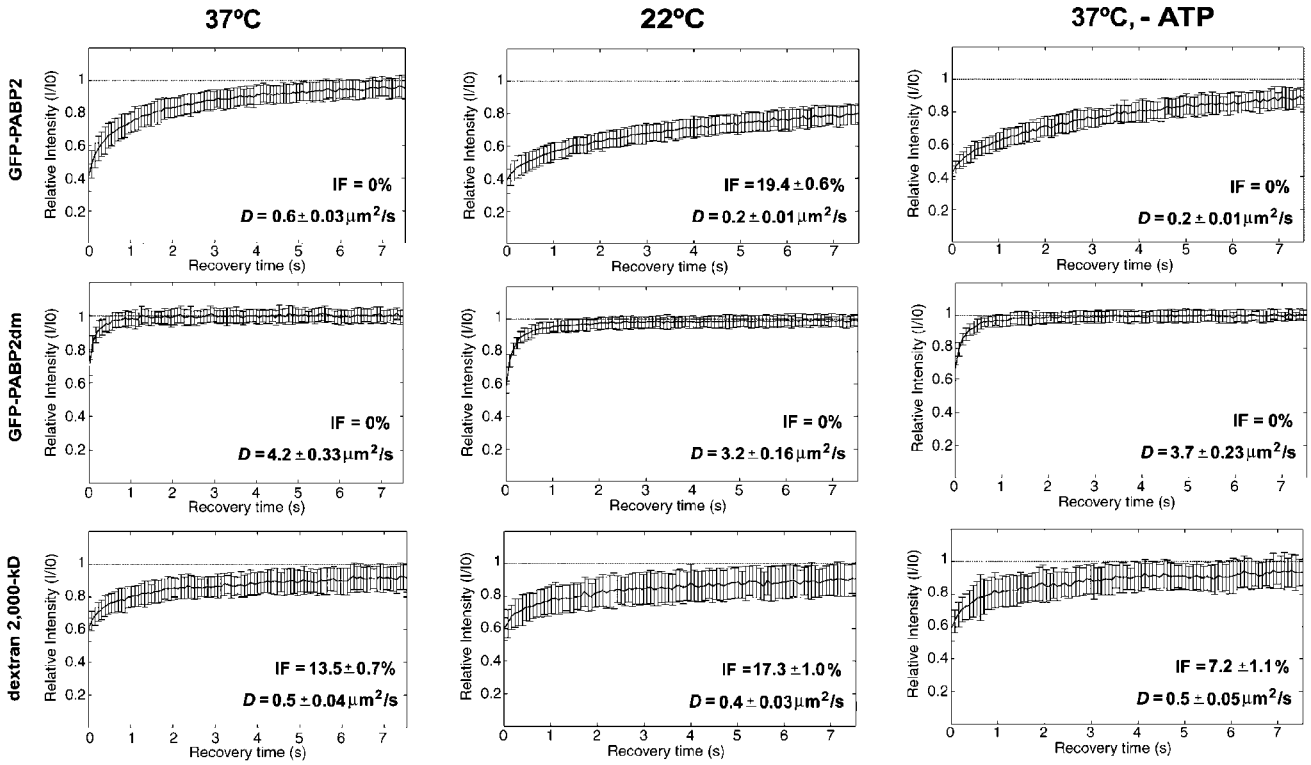

Figure 8. **Recovery of GFP–PABP2 is ATP dependent and temperature sensitive.** Cells expressing GFP–PABP2 or GFP–PABP2dm, or microinjected with FITC–dextrans were incubated at either 37°C or 22°C, or treated with 2-deoxy-D-glucose and sodium azide to lower the cellular levels of ATP. The recovery curves correspond to a pool of three to five independent experiments, with 10 different cells analyzed per experiment. Error bars represent standard deviations. IF, immobile fraction. *D* values represent mean ± SEM.

of the large dextran and reduced that of GFP–PABP2dm to ~90% of the control value. Thus, although energy-depleting treatments do reduce the mobility of both the large dextran and the PABP2 mutant with impaired ability to bind RNA, the effect is significantly more drastic on wild-type PABP2.

The next question to be addressed was whether energy depletion affects the binding of PABP2 to poly(A) RNA. This was examined by using an electrophoretic mobility shift assay with ^{32}P-labeled poly(A) (A_{250}). As depicted in Fig. 9, addition of a 1,000-fold molar excess of unlabeled substrate completely displaced PABP2 from radioactive poly(A) (A_{250}). The displacement occurs within seconds after addition of the unlabeled competitor, in the absence of ATP or any other source of energy. Furthermore, similar results were obtained when the assay was performed at either 37°C or 22°C (unpublished data). These results show that in vitro PABP2 is constantly exchanging between poly(A) substrates in a process that is independent of energy.

The mobility of GFP–PABP2 is not affected by a short treatment with actinomycin D

Several recent lines of evidence indicate that export of mRNA to the cytoplasm is tightly coupled to cotranscriptional processing of newly synthesized pre-mRNAs in the nucleus (Kataoka et al., 2000; Zhou et al., 2000; Lei et al., 2001). Thus, because both transcription and pre-mRNA splicing are ATP dependent, the FRAP results obtained in

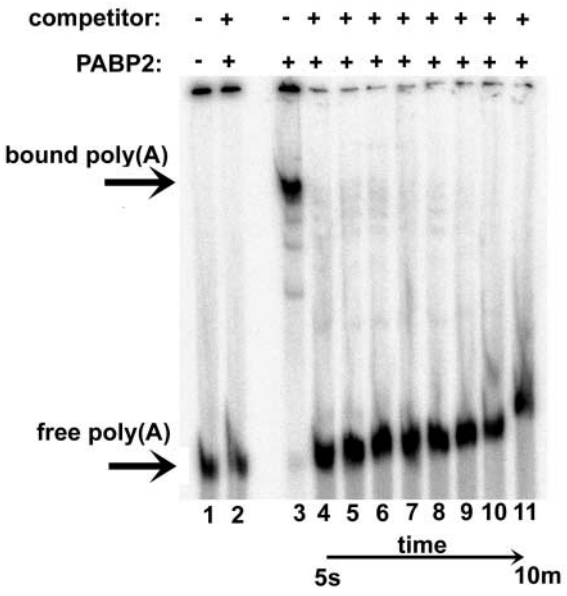

Figure 9. **Binding of PABP2 to poly(A) in vitro does not require energy.** Binding of PABP2 to oligo (A_{250}) was analyzed by an electrophoretic mobility shift assay. PABP2 (10 nM) was incubated at 37°C with ^{32}P-labeled A_{250} for 30 min and further incubated with 10 μM unlabeled oligonucleotide for the indicated time periods, in the absence of ATP or any other source of energy. Samples were placed while the gel was running.

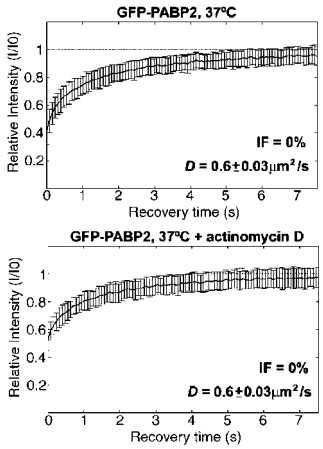

Figure 10. **Recovery of GFP–PABP2 is not affected by actinomycin D.** Cells expressing GFP–PABP2 were either nontreated or treated with actinomycin D for 30–60 min before FRAP analysis. Each recovery curve corresponds to a pool of four independent experiments, with 10 different cells analyzed per experiment. Error bars represent standard deviations. IF, immobile fraction. *D* values represent mean ± SEM.

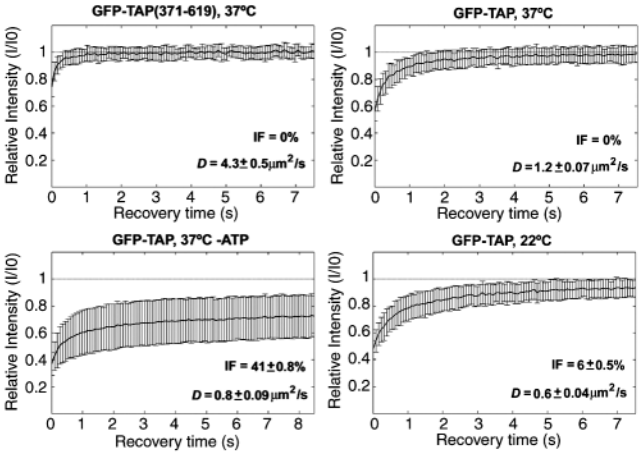

Figure 11. **Kinetics of GFP–TAP.** FRAP was performed on cells expressing GFP–TAP 371–619 or GFP–TAP. Cells expressing GFP–TAP were incubated at either 37°C or 22°C, or treated with 2-deoxy-D-glucose and sodium azide to lower the cellular levels of ATP. The recovery curves correspond to a pool of three independent experiments, with 10 different cells analyzed per experiment. Error bars represent standard deviations. IF, immobile fraction. *D* values represent mean ± SEM.

energy-depleted cells could be caused by inhibition of these two processes. To address this issue, FRAP experiments were performed on cells treated for 30–60 min with the transcription inhibitor actinomycin D. The results show recovery kinetics similar to that detected in nontreated cells (Fig. 10). However, longer periods of incubation with actinomycin D resulted in a progressive immobilization of both GFP–PABP2 and other GFP-tagged nuclear proteins (unpublished data), suggesting that prolonged treatment with actinomycin D causes a general obstruction to macromolecular mobility due to alterations in the intranuclear environment.

It is well known that actinomycin D treatment does not deplete the HeLa cell nucleus of poly(A) RNA (Huang et al., 1994). Thus, it is expected that GFP–PABP2 molecules remain bound to poly(A) RNP complexes synthesized before the inhibition of transcription. The similar recovery kinetics observed for GFP–PABP2 in untreated and treated cells therefore suggests that the mobility of poly(A) RNPs is not significantly affected in actinomycin D–treated cells. This indicates that on-going transcription is not essential for the movement of previously synthesized mRNP complexes in the nucleus.

Energy-dependent mobility of GFP–TAP

Next, photobleaching experiments were performed using a GFP-tagged version of the mRNA export factor TAP. TAP associates with cellular mRNPs and is thought to promote their export by interacting with nuclear pore proteins during translocation (Bachi et al., 2000). The NH_2-terminal region of the TAP protein includes a noncanonical RNP-type RNA binding domain that exhibits general RNA binding activity (Liker et al., 2000) and four leucine-rich repeats, which play an essential role in TAP-mediated export of mRNA (Braun et al., 2001).

A TAP fragment comprising residues 371–619 (which excludes both the RNA binding domain and the leucine-rich repeats; Bachi et al., 2000) was fused to GFP and used in photobleaching experiments (Fig. 11). The recovery curve shows that this protein moves with kinetics similar to that of GFP–PABP2dm (*D* values of 4.3 and 4.2 $\mu m^2 s^{-1}$, respectively), suggesting that it does not assemble into a larger macromolecular complex. In contrast, the fluorescence recovery of GFP fused to full-length TAP was significantly slower ($D = 1.2\ \mu m^2 s^{-1}$), as expected from its binding to mRNP complexes. Compared with the diffusion coefficient of GFP–PABP2 ($0.6\ \mu m^2 s^{-1}$), GFP–TAP has a faster diffusion rate. FLIP analysis shows that this apparent higher mobility is caused by the presence of two distinct GFP–TAP populations in the nucleus, a slow-moving fraction of molecules bound to mRNP complexes and a fast-moving population of unbound molecules (to be described in detail elsewhere). In contrast, GFP–PABP2 forms a single population of molecules, the vast majority of which are bound to poly(A) RNPs (Fig. 5).

When cells were either ATP depleted or incubated at 22°C, the fluorescence recovery of GFP–TAP became slower and the immobile fractions increased (Fig. 11). The diffusion coefficients decreased from 1.2 $\mu m^2 s^{-1}$ to 0.8 and 0.6 $\mu m^2 s^{-1}$, respectively. Thus, as observed for GFP–PABP2, energy depletion significantly reduces the mobility of GFP–TAP molecules presumably bound to mRNP complexes.

Discussion

In this work, we analyzed the mobility of GFP-tagged RNP complexes in the nucleus of living HeLa cells using photobleaching techniques. Bulk RNPs containing poly(A) RNA were visualized with GFP–PABP2. In addition, GFP–TAP was used to tag export-competent mRNP complexes. The main conclusion is that the GFP-tagged RNP complexes diffuse freely in the nucleus, whereas a large dextran, the size of which corresponds approximately to 40S mRNP particles, is partially immobilized. In addition, energy depletion reduces the intranuclear mobility of wild-type GFP–

PABP2 and GFP–TAP significantly, as compared with the large dextran and a GFP–PABP2 mutant with impaired ability to bind to RNA. This suggests that although mRNPs diffuse in the nucleus, energy-dependent processes contribute to enhance their mobility.

Here we estimated a diffusion coefficient of 0.6 ± 0.03 $\mu m^2 s^{-1}$ for RNP complexes containing GFP–PABP2 in the nucleus. A very similar value (0.6 ± 0.1 $\mu m^2 s^{-1}$) was reported by Politz et al. (1999) using fluorescein-labeled oligo(dT) hybridized to nuclear poly(A) RNA. The diffusion coefficient for a particle in a solution is given by the Stokes-Einstein formula, $D = kT/6\pi\eta R_h$, which correlates the hydrodynamic behavior of a sphere with the absolute temperature T, the viscosity of the solution η, the Boltzmann constant k, and the hydrodynamic radius of the particle R_h (for a recent review see Reits and Neefjes, 2001). Because viscosity is highly dependent on temperature, this equation implies that changes in diffusion coefficients are expected in response to temperature variation. Because the viscosity of water increases ~30% when temperature is lowered from 37°C to 22–23°C, the diffusion coefficient for a particle in the nucleus should decrease by a similar order of magnitude. Consistent with this prediction, we observe a reduction of ~25% in the diffusion coefficients of the 2,000-kD dextran and the mutant form of PABP2 when the temperature is lowered from 37°C to 22°C. Likewise, an ~30% reduction in recovery rate was reported for soluble GFP targeted to the endoplasmic reticulum when FRAP experiments were performed at 37°C and 23°C (Reits and Neefjes, 2001). In contrast to these results, other studies did not detect a significant effect of reducing the temperature to 23°C on the mobility rate of either GFP-tagged nuclear proteins (Phair and Misteli, 2000) or nuclear poly(A) RNA hybridized with fluorescein-labeled oligo(dT) (Politz et al., 1999).

Contrasting to the observed ~25% reduction in the recovery rates of both the large dextran and the RNA binding–deficient GFP–PABP2 mutant, lowering the temperature from 37°C to 22°C caused an ~60% reduction in the diffusion coefficient of wild-type GFP–PABP2, and a similar effect was observed after depleting the cells of ATP. Thus, energy-depleting treatments act specifically on the mobility of the fusion protein that binds to poly(A) RNA, arguing against a general effect caused by an alteration of the intranuclear environment induced by these treatments. Using a very different technical approach, Politz et al. (1999) measured the movement of nuclear poly(A) RNA and estimated the same apparent diffusion coefficient at both 37°C and 23°C. The method devised by these authors consisted of hybridizing chemically masked (caged) fluorescein to poly(A) RNA, using laser spot photolysis to uncage the fluorochrome, and measuring the radial distance that the signal traveled from the uncaging site. The radial movement of signal was calculated and plotted over time, and the diffusion coefficient was estimated from the slope of the unweighted least-squares fit line (Politz et al., 1999). The different methods used for both poly(A) RNA visualization and quantitative analysis are probably on the basis of the discrepancy between the conclusions of this earlier study and our present data.

Although the mechanism underlying the movement of poly(A) RNPs within the nucleus remains unknown, a parallel can de drawn with the process of translocation through the nuclear pore complex. Early studies showed that energy depletion blocked nuclear import and arrested the molecules in transit at the nuclear pore complexes (Newmeyer and Forbes, 1988; Richardson et al., 1988). Later, GTP hydrolysis by Ran was shown to drive transport, presumably by powering the actual translocation through the pore. However, more recent evidence revealed that the translocation step, per se, is not directly coupled to GTP hydrolysis. Rather, it appears that the translocation process occurs by facilitated diffusion, at least for relatively small cargoes (for review see Görlich and Kutay, 1999). According to this view, it has been proposed that energy depletion inhibits nuclear import by blocking the terminal release of molecules in transit from the nuclear pore into the nucleoplasm (Ribbeck and Görlich, 2001).

Although at present the mechanistic details involved in mRNP traffic inside the nucleus are completely unknown, one possibility is that in order to escape immobilization imposed by the densely packed nuclear interior, mRNPs rely on ATP-dependent enzymatic activities. Putative candidates to maintain mRNP particles in a mobile state are ATP-dependent RNA helicases, such as Dbp5p, which participates in the export of mRNAs out of the nucleus (Schmitt et al., 1999; Strahm et al., 1999). Although Dbp5p was first predominantly detected in the cytoplasmic side of nuclear pore complexes, a recent study shows that in *C. tentans*, this helicase binds mRNPs cotranscriptionally and accompanies the particle to the pores (Zhao et al., 2002). Additional candidates include actin-related ATPases and actomyosin-based molecular motors. A nuclear isoform of myosin I has been recently identified in a complex with RNA polymerase II (Pestic-Dragovich et al., 2000), and it is well established that mRNAs in the cytoplasm can be transported by an actomyosin-driven mechanism (Long et al., 1997; Takizawa et al., 1997). Furthermore, an increasing number of reports describe the association of actin and/or actin-related proteins (Arps) with chromatin complexes (for review see Boyer and Peterson, 2000). Actin has also been found associated with Balbiani ring mRNA (Percipalle et al., 2001) and with the nucleoplasmic filaments of nuclear pore complexes (Hofmann et al., 2001), thus suggesting an involvement in the RNA export pathway. The experimental approach described in this study should be applicable for future screening and identification of proteins that play a role in the intranuclear mobility of mRNP complexes.

Materials and methods

Cell culture, transfection, and microinjection

HeLa cells were cultured as monolayers in DME supplemented with 10% FCS (GIBCO BRL). Cells were plated and observed in glass bottom chambers (MatTek Corporation). For imaging, the medium was changed to DME/F-12 without phenol red supplemented with 15 mM Hepes buffer (GIBCO BRL).

All GFP fusion constructs were obtained by subcloning into the appropriate pEGFP-C vector (CLONTECH Laboratories, Inc.). We have previously described the construction and properties of GFP–PABP2 and GFP–PABP2dm (Calado and Carmo-Fonseca, 2000; Calado et al., 2000). GFP–TAP and GFP–TAP 371–619 were also previously described (Bachi et al., 2000). The pEGFP-coilin–PABP2 plasmid was constructed by subcloning the cDNA of coilin into the pEGFP-PABP2 vector. The cDNA of coilin was obtained from pBluescript SK(−) coilin (Bohmann et al., 1995)

through restriction with BamHI and PvuII and purification with the Qiaex II kit (QIAGEN). This double restriction deletes the DNA sequence that encodes for the 108 COOH-terminal amino acids of coilin. As a result, PABP2 is fused to a COOH-terminally truncated form of coilin. The pEGFP-PABP2 vector was first restricted with Sal I and the protruding ends generated were filled in. This vector was then restricted with Bgl II and ligated to the coilin-coding fragment. DNA for transfection was purified using the plasmid DNA midiprep kit (QIAGEN). HeLa cells were transfected with FuGene6 reagent (Roche Biochemicals) using 1 μg of DNA and analyzed 16–24 h after transfection. FITC-labeled dextrans with average molecular sizes of 580 and 2,000 kD (Sigma-Aldrich) were diluted to 200 μg/ml in water and microinjected into the nucleus of HeLa cells as previously described (Almeida et al., 1998). Actinomycin D (Sigma-Aldrich) was used at 5 μg/ml from a stock solution of 5 mg/ml in DMSO. A stock solution of 0.6 M 2-deoxy-D-glucose was prepared in water and sodium azide was used from a 1 M stock solution freshly prepared in DME/F-12. Energy depletion experiments were performed by incubating cells in 12 mM 2-deoxy-D-glucose and 20 mM sodium azide for 30–60 min at 37°C. To stain selectively active mitochondria, the cells were incubated with rhodamine 123 (Molecular Probes) for 5–10 min.

Cellular fractionation and immunoprecipitation

Immunopurification of hnRNP complexes from HeLa cells transfected with pEGFP-PABP2 or pEGFP-PABP2dm was performed according to Piñol-Roma et al. (1990). In brief, cells were rinsed twice with cold PBS, scraped with a rubber policeman into 1 ml of cold immunopurification buffer (IPB), and lysed by passing through a 25-gauge needle. The nuclei were pelleted, resuspended in 500 μl IPB, disrupted by sonicating, and layered in an equal volume of 30% sucrose cushion. After centrifugation at 4,000 *g* for 15 min at 4°C to remove nucleoli, chromatin, and other insoluble nuclear structures, the nucleoplasm-enriched fraction that overlays the cushion was collected. When required, RNase A was directly added onto this fraction at the final concentration of 100 μg/ml and digestion was allowed to proceed at 30°C for 10 min (Piñol-Roma, 1999).

Prior to immunoprecipitation, anti–hnRNP C (4F4; Choi and Dreyfuss, 1984) or anti-GFP (Roche Biochemicals) monoclonal antibodies were covalently conjugated to protein A–Sepharose beads (CL-4B; Amersham Biosciences) or protein G–Sepharose beads (Sigma-Aldrich), respectively. For the immunoprecipitation, 25 μl (packed volume) of beads were used for each 10-cm plate. The beads were first washed with IPB and then incubated with the nucleoplasmic fraction for 10 min at 4°C with rocking. After washing, the immunoprecipitation complexes were eluted by boiling the beads in SDS-PAGE sample buffer. Immunoprecipitates were analyzed by Western blotting using anti–hnRNP C and anti-GFP antibodies. SDS-PAGE and Western blotting were performed as previously described (Almeida et al., 1998).

Electrophoretic mobility shift assay

A radiolabeled probe was synthesized by 5′ end labeling of an A_{250} oligonucleotide with [γ-^{32}P]ATP using T4 polynucleotide kinase (Fermentas). PABP2 was purified from calf thymus as previously described (Wahle et al., 1993). 10 nM ^{32}P-labeled A_{250} probe was mixed with an equimolar amount of PABP2 diluted in 50 mM Tris (pH 8.0), 100 mM KCl, 10% glycerin, 0.5 mM DTT, 0.01% NP-40, 0.2 mg/ml BSA, 2.6% PVA, and 2 mM $MgCl_2$ and incubated for 30 min at either 37°C or room temperature (22°C). A 1,000-fold excess (10 μM) of unlabeled A_{250} oligonucleotide was then added to the mix. Aliquots were removed at the indicated times and directly loaded onto the running gel. Complexes were resolved by electrophoresis through nondenaturing 6% polyacrylamide gels (80:1 acrylamide/bisacrylamide ratio). Gels were run at 4°C for 2 h at 20 V/cm and analyzed using the Molecular Dynamics PhosphorImager.

Confocal microscopy and image analysis

Live cells were imaged at 37°C or 22°C, maintained by a heating/cooling frame (LaCon GbR) in conjunction with an objective heater (PeCon GmbH). Images were acquired on a ZEISS LSM 510 with the planapochromat 63x/1.4 objective. EGFP fluorescence was detected using the 488-nm laser line of an Ar laser (25 mW nominal output) in conjunction with an LP 505 filter. Each FRAP analysis started with three image scans, followed by a single bleach pulse of 37 ms on a spot with a diameter of 25 pixels (0.71-μm radius). A series of 97 single-section images were then collected at 78-ms intervals, with the first image acquired 2 ms after the end of bleaching. Image size was 512 × 50 pixels and the pixel width was 57 nm. For imaging, the laser power was attenuated to 0.1–0.2% of the bleach intensity.

For each time series, the background and nuclear regions were identified using an implementation of the ICM segmentation algorithm (Besag, 1986; Fwu and Djuriç, 1996) in Mathworks Matlab software. The average fluorescence in the nucleus $T(t)$ and the average fluorescence in the bleached region $I(t)$ were calculated for each background-subtracted image at time t after bleaching. FRAP recovery curves were normalized according to Phair and Misteli (2000),

$$Irel(t) = \frac{I(t)}{I_i}\frac{T_i}{T(t)},$$

where T_i is the fluorescence in the nucleus before bleaching and I_i is the fluorescence in the bleached region before bleaching. This normalization corrects for the loss of fluorescence caused by imaging. Typically, ~10% of the total EGFP or FITC fluorescence was lost during the bleach pulse. During the post-bleaching scanning phase, the fluorescence lost was <5% for EGFP and 15–17% for FITC.

Quantitative FRAP analysis

Nucleoplasmic diffusion coefficients were determined essentially as described previously (Axelrod et al., 1976; Phair and Misteli, 2000). We assume that fluorescent molecules can be either mobile (with a diffusion coefficient D) or immobile. The initial concentration of fluorophore inside the bleached zone is C_0, γ being the percentage of immobile molecules (ranging from 0 to 1). Total fluorescence observed inside the bleached spot is then the sum of the fluorescence of the mobile molecules and the fluorescence of the immobile ones. After bleach, the immobile fraction fluorescence is constant inside the bleached spot (Axelrod et al., 1976):

$$F_{im}(t) = \kappa C_0 \gamma \frac{1 - e^{-K}}{K},$$

where K is the bleach constant and κ is a parameter that depends on the properties of the laser and of the detection system. The mobile fraction fluorescence is given by

$$F_m(t) = \kappa C_0 (1-\gamma) \sum_{n=0}^{+\infty} \frac{(-K)^n}{n!}\left(1 + n\left(1 + 2\frac{t}{\tau_D}\right)\right)^{-1}$$

(Axelrod et al., 1976), where τ_D is the characteristic time of diffusion and is related with the diffusion coefficient by $D = w^2/4\tau_D$. The total normalized fluorescence is then

$$Irel^*(t) = (1-\gamma) \sum_{n=0}^{+\infty} \frac{(-K)^n}{n!}\left(1 + n\left(1 + 2\frac{t}{\tau_D}\right)\right)^{-1} + \gamma\frac{1 - e^{-K}}{K},$$

i.e., the normalized fluorescence is just the weighted sum of the fluorescence recovery of the mobile portion of the fluorophore (first term) and the fluorescence after bleaching of the immobile portion of the fluorophore (second term).

The bleaching characteristics of the laser were estimated using fixed cells expressing GFP. The post-bleaching concentration of fluorophore at distance r from the center of the bleached region was fitted to a Gaussian laser profile (Axelrod et al., 1976),

$$C(r) = \exp\left(-k\exp\left(-2\frac{r^2}{w^2}\right)\right),$$

where k is the bleach constant for the fixed cells and w is half the width of the laser beam at $1/e^2$ intensity. Nonlinear regression in Mathematica yielded $k = 2.14 \pm 0.06$ and $w = 1.13 \pm 0.01$ μm (mean ± SEM). The FRAP recovery curves were then fitted to the recovery function, $Irel^*(t)$.

The series solution for the fluorescence recovery was truncated after 40 terms (Phair and Misteli, 2000), assuring that neglected terms made an insignificant contribution. We estimated the bleach constant, the immobile fraction, and the characteristic diffusion time for each set of FRAP replicates using a weighted least squares algorithm (Bell et al., 1996) implemented in Mathematica (WOLFRAM Research).

FLIP analysis

For FLIP experiments, cells were repeatedly bleached at intervals of 3.5 s and imaged between bleach pulses. Bleaching was performed by 278-ms bleach pulses on a spot with a diameter of 35 pixels (2.1-μm radius). Repetitive bleach pulses were achieved by taking advantage of the trigger interface for LSM 510. An electronic oscillator circuit was built to create pulses with a user-defined frequency. When connected to the LSM 510, it would then trigger the bleaching events. A series of 350 images was collected for each cell with laser power attenuated to 1% of the bleach inten-

sity. Nuclear fluorescence of selected areas in FLIP experiments was measured using the ROI mean function of the LSM 510 physiology package. The data were then background subtracted and normalized to correct the loss of fluorescence caused by imaging, in a way similar to FRAP, but using an adjacent cell to estimate $T(t)$ and T_0. Loss of fluorescence due to imaging could reach 20–25% over the time course of the experiment.

Nuclear fluorescence data from FLIP experiments was fitted to a single exponential with rate constant R (Fig. 5 A) and to a nonlinear curve corresponding to the sum of two exponentials,

$$f(t) = p\exp(-R_1 t) + (1-p)\exp(-R_2 t),$$

where p is the proportion of the slower population relative to the total fluorescence, R_1 is the rate constant associated with this slower population, and R_2 the rate constant of the faster one (Fig. 5, B and C). The optimal fit for each case was chosen according to its chi-square value.

We thank Tom Misteli for stimulating discussions and critical comments. We further wish to acknowledge Rainer Pepperkok, Ernst Stelzer, and Jan Ellenberg for help with FRAP analysis, Serafin Piñol-Roma for advice on immunopurification of hnRNP complexes, and Inês Condado, Helena Pina, and Maria do Carmo Silva for technical support. We are also thankful to Elisa Izaurralde (EMBL, Heidelberg, Germnay) for providing GFP–TAP and GFP–TAP 371-619, and Gideon Dreyfuss (University of Pennsylvania, College Park, PA) for mAb 4F4.

This study was supported by Fundação para a Ciência e Tecnologia, Portugal, and by the European Commission (contract BMH4-98-3147). A. Calado was a fellow from the Gulbenkian PhD program.

Submitted: 11 March 2002
Revised: 29 October 2002
Accepted: 31 October 2002

References

Agutter, P.S., and P.L. Taylor. 1996. The meaning of nucleocytoplasmic transport. Medical Intelligence Unit Series. R.G. Landes Company and Chapman & Hall, Austin, Texas.

Almeida, F., R. Saffrich, W. Ansorge, and M. Carmo-Fonseca. 1998. Microinjection of anti-coilin antibodies affects the structure of coiled bodies. *J. Cell Biol.* 142:899–912.

Axelrod, D., D.E. Koppel, J. Schlessinger, E. Elson, and W.W. Webb. 1976. Mobility measurement by analysis of fluorescence photobleaching recovery kinetics. *Biophys. J.* 16:1055–1069.

Bachi, A., I.C. Braun, J.P. Rodrigues, N. Panté, K. Ribbeck, C. von Kobbe, U. Kutay, M. Wilm, D. Görlich, M. Carmo-Fonseca, and E. Izaurralde. 2000. The C-terminal domain of TAP interacts with the nuclear pore complex and promotes export of specific CTE-bearing RNA substrates. *RNA.* 6:136–158.

Bauren, G., S. Belikov, and L. Wieslander. 1998. Transcriptional termination in the Balbiani ring 1 gene is closely coupled to 3′-end formation and excision of the 3′-terminal intron. *Genes Dev.* 12:2759–2769.

Bell, B.M., J.V. Burke, and A. Schumitsky. 1996. A relative weighting method for estimating parameters and variances in multiple data sets. *Computational Statistics and Data Analysis.* 22:119–135.

Besag, J. 1986. On the statistical analysis of dirty pictures. *Journal of the Royal Statistical Society: Series B.* 48:259–302.

Beyer, A.L., M.E. Christensen, B.W. Walker, and W.M. Le Stourgeon. 1977. Identification and characterization of the packaging proteins of core 40S hnRNP particles. *Cell.* 11:127–138.

Blobel, G. 1985. Gene gating: a hypothesis. *Proc. Natl. Acad. Sci. USA.* 82:8527–8529.

Bohmann, K., J. Ferreira, and A.I. Lamond. 1995. Mutational analysis of p80 coilin indicates a functional interaction between coiled bodies and nucleolus. *J. Cell Biol.* 131:817–831.

Boyer, L.A., and C.L. Peterson. 2000. Actin-related proteins (Arps): conformational switches for chromatin-remodeling machines? *Bioessays.* 22:666–672.

Braun, I.C., A. Herold, M. Rode, E. Conti, and E. Izaurralde. 2001. Overexpression of TAP/p15 heterodimers bypasses nuclear retention and stimulates nuclear mRNA export. *J. Biol. Chem.* 276:20536–20543.

Calado, A., and M. Carmo-Fonseca. 2000. Localization of poly(A)-binding protein 2 (PABP2) in nuclear speckles is independent of import into the nucleus and requires binding to poly(A)RNA. *J. Cell Sci.* 113:2309–2318.

Calado, A., U. Kutay, U. Kühn, E. Wahle, and M. Carmo-Fonseca. 2000. Deciphering the cellular pathway for transport of poly(A)-binding protein II. *RNA.* 6:245–256.

Choi, Y.D., and G. Dreyfuss. 1984. Monoclonal antibody characterization of the C proteins of heterogeneous nuclear ribonucleoprotein complexes in vertebrate cells. *J. Cell Biol.* 99:1997–2004.

Conti, E., and E. Izaurralde. 2001. Nucleocytoplasmic transport enters the atomic age. *Curr. Opin. Cell Biol.* 13:310–319.

Derman, E., S. Goldberg, and J.E. Darnell. 1976. hnRNA in HeLa cells: distribution of transcript sizes estimated from nascent molecule profile. *Cell.* 9:465–472.

Dreyfuss, G., M.J. Matunis, S. Piñol-Roma, and C.G. Burd. 1993. hnRNP proteins and the biogenesis of mRNA. *Annu. Rev. Biochem.* 62:289–321.

Dye, M.J., and N.J. Proudfoot. 1999. Terminal exon definition occurs cotranscriptionally and promotes termination of RNA polymerase II. *Mol. Cell.* 3:371–378.

Dye, M.J., and N.J. Proudfoot. 2001. Multiple transcript cleavage precedes polymerase release in termination by RNA polymerase II. *Cell.* 105:669–681.

Fwu, J.K., and P.M. Djuriç. 1996. Unsupervised vector image segmentation by a tree structure-ICM algorithm. *IEEE Transactions on Medical Imaging.* 15: 871–880.

Georgiev, G.P. 1981. Precursor of mRNA (pre-mRNA) and ribonucleoprotein particles containing pre-mRNA. *In* The Cell Nucleus. Vol. 4. H. Busch, editor. Academic Press Inc., New York. 67–108.

Görlich, D., and U. Kutay. 1999. Transport between the cell nucleus and the cytoplasm. *Annu. Rev. Cell Dev. Biol.* 15:607–660.

Hofmann, W., B. Reichart, A. Ewald, E. Muller, I. Schmitt, R.H. Stauber, F. Lottspeich, B.M. Jockusch, U. Scheer, J. Hauber, and M.C. Dabauvalle. 2001. Cofactor requirements for nuclear export of Rev response element (RRE)– and constitutive transport element (CTE)–containing retroviral RNAs. An unexpected role for actin. *J. Cell Biol.* 152:895–910.

Huang, S., T.J. Deerinck, M.H. Ellisman, and D.L. Spector. 1994. In vivo analysis of the stability and transport of nuclear poly(A)$^+$ RNA. *J. Cell Biol.* 126: 877–899.

Kataoka, N., J. Yong, V.N. Kim, F. Velazquez, R.A. Perkinson, F. Wang, and G. Dreyfuss. 2000. Pre-mRNA splicing imprints mRNA in the nucleus with a novel RNA-binding protein that persists in the cytoplasm. *Mol. Cell.* 6:673–682.

Krause, S., S. Fakan, K. Weis, and E. Wahle. 1994. Immunodetection of poly(A)-binding protein II in the cell nucleus. *Exp. Cell Res.* 214:75–82.

Lei, E.P., H. Krebber, and P.A. Silver. 2001. Messenger RNAs are recruited for nuclear export during transcription. *Genes Dev.* 15:1771–1782.

Liker, E., E. Fernandez, E. Izaurralde, and E. Conti. 2000. The structure of the mRNA export factor TAP reveals a cis arrangement of a non-canonical RNP domain and an LRR domain. *EMBO J.* 19:5587–5598.

Long, R.M., R.H. Singer, X. Meng, I. Gonzalez, K. Nasmyth, and R.-P. Jansen. 1997. Mating type switching in yeast controlled by asymmetric localization of ASH1 mRNA. *Science.* 277:383–387.

Maquat, L.E., and G.G. Carmichael. 2001. Quality control of mRNA function. *Cell.* 104:173–176.

Nakielny, S., and G. Dreyfuss. 1999. Transport of proteins and RNAs in and out of the nucleus. *Cell.* 99:677–690.

Nemeth, A., S. Krause, D. Blank, A. Jenny, P. Jenö, A. Lustig, and E. Wahle. 1995. Isolation of genomic and cDNA clones encoding poly(A) binding protein II. *Nucleic Acids Res.* 23:4034–4041.

Newmeyer, D.D., and D.J. Forbes. 1988. Nuclear import can be separated into distinct steps in vitro, nuclear pore binding and translocation. *Cell.* 52:641–653.

Pederson, T. 1974. Proteins associated with heterogeneous nuclear RNA in eukaryotic cells. *J. Mol. Biol.* 83:163–183.

Percipalle, P., J. Zhao, B. Pope, A. Weeds, U. Lindberg, and B. Daneholt. 2001. Actin bound to the heterogeneous nuclear ribonucleoprotein hrp36 is associated with Balbiani ring mRNA from the gene to polysomes. *J. Cell Biol.* 153: 229–236.

Pestic-Dragovich, L., L. Stojiljkovic, A.A. Philimonenko, G. Nowak, Y. Ke, R.E. Settlage, J. Shabanowitz, D.F. Hunt, P. Hozak, and P. de Lanerolle. 2000. A myosin I isoform in the nucleus. *Science.* 290:337–341.

Phair, R.D., and T. Misteli. 2000. High mobility of proteins in the mammalian cell nucleus. *Nature.* 404:604–609.

Piñol-Roma, S. 1999. Association of nonribosomal nucleolar proteins in ribonucleoprotein complexes during interphase and mitosis. *Mol. Biol. Cell.* 10:77–90.

Piñol-Roma, S., Y.D. Choi, and G. Dreyfuss. 1990. Immunological methods for purification and characterization of heterogeneous nuclear ribonucleoprotein complexes. *Methods Enzymol.* 181:317–325.

Politz, J.C., E.S. Browne, D.E. Wolf, and T. Pederson. 1998. Intranuclear diffusion and hybridization state of oligonucleotides measured by fluorescence correlation spectroscopy in living cells. *Proc. Natl. Acad. Sci. USA.* 95:6043–6048.

Politz, J.C., R.A. Tuft, T. Pederson, and R. Singer. 1999. Movement of nuclear

poly(A) RNA throughout the interchromatin space in living cells. *Curr. Biol.* 9:285–291.

Reits, E.A.J., and J.J. Neefjes. 2001. From fixed to FRAP: measuring protein mobility and activity in living cells. *Nat. Cell Biol.* 3:E145–E147.

Ribbeck, K., and D. Görlich. 2001. Kinetic analysis of translocation through nuclear pore complexes. *EMBO J.* 20:1320–1330.

Richardson, W.D., A.D. Mills, S.M. Dilworth, R.A. Laskey, and C. Dingwall. 1988. Nuclear protein migration involves two steps: rapid binding at the nuclear envelope followed by slower translocation through nuclear pores. *Cell.* 52:655–664.

Schmitt, C., C. von Kobbe, A. Bachi, N. Pante, J.P. Rodrigues, C. Boscheron, G. Rigaut, M. Wilm, B. Seraphin, M. Carmo-Fonseca, and E. Izaurralde. 1999. Dbp5, a DEAD-box protein required for mRNA export, is recruited to the cytoplasmic fibrils of nuclear pore complex via a conserved interaction with CAN/Nup159p. *EMBO J.* 18:4332–4347.

Seksek, O., J. Biwersi, and A.S. Verkam. 1997. Translational diffusion of macromolecule-sized solutes in cytoplasm and nucleus. *J. Cell Biol.* 138:131–142.

Singh, O.P., B. Björkroth, S. Masich, L. Wieslander, and B. Daneholt. 1999. The intranuclear movement of Balbiani ring pre-messenger ribonucleoprotein particles. *Exp. Cell Res.* 251:135–146.

Strahm, Y., B. Fahrenkrog, D. Zenklusen, E. Rychner, J. Kantor, M. Rosbach, and F. Stutz. 1999. The RNA export factor Gle1p is located on the cytoplasmic fibrils of the NPC and physically interacts with the FG-nucleoporin Rip1p, the DEAD-box protein Rat8p/Dbp5p and a new protein Ymr 255p. *EMBO J.* 18:5761–5777.

Takizawa, P.A., A. Sil, J.R. Swedlow, I. Herskowitz, and R.D. Vale. 1997. Actin-dependent localization of an RNA encoding a cell fate determinant in yeast. *Nature.* 389:90–93.

Wahle, E. 1991. A novel poly(A)-binding protein acts as a specificity factor in the second phase of messenger RNA polyadenylation. *Cell.* 66:759–768.

Wahle, E., A. Lustig, P. Jeno, and P. Maurer. 1993. Mammalian poly(A)-binding protein II. Physical properties and binding to polynucleotides. *J. Biol. Chem.* 268:2937–2945.

White, J., and E. Stelzer. 1999. Photobleaching GFP reveals protein dynamics inside live cells. *Trends Cell Biol.* 9:61–65.

Zhao, J., S.B. Jin, B. Bjorkroth, L. Wieslander, and B. Daneholt. 2002. The mRNA export factor Dbp5 is associated with Balbiani ring mRNP from gene to cytoplasm. *EMBO J.* 21:1177–1187.

Zhou, Z., M.-J. Luo, K. Straesser, J. Katahira, E. Hurt, and R. Reed. 2000. The protein Aly links pre-messenger-RNA splicing to nuclear export in metazoans. *Nature.* 407:401–405.